

CFD Modelling of Natural Convection in Air Cavities

Yingchun Ji^{1c}

¹ School of the Built Environment, University of Salford, U.K

Received: 06/08/2013 – Revised 25/12/2013 – Accepted 03/02/2014

Abstract

This paper discusses the modelling of natural convection in air cavities using four eddy viscosity turbulence models. Two 2D closed cavities with differentially heated walls opposite each other and one 3D open ended tall cavity with one side is heated and adiabatic for all the others were investigated. The CFD simulation results for the two 2D cases were compared with their corresponding experimental measurements and it was found that the k-omega turbulence model offered the best solution among the turbulence models tested. Close agreement was also achieved between the k-omega model and the experiments in the prediction of temperature and velocity fields for the 3D case with Monte Carlo radiation model. The work has demonstrated the ability of the eddy viscosity turbulence models for modelling natural convection and radiation in different types of cavities.

Keywords: Cavity; Natural Convection; Radiation; Turbulence model; CFD.

1. Introduction

Natural convection in air cavities has been the subject of much research in recent decades due to its various engineering applications, such as solar chimneys, double skin façades, and Trombe walls. Understanding the underlying flow characteristics of these types of engineering applications are important for engineers and architects to design low energy ventilation, cooling and heating for buildings [1]. It is difficult to analytically solve natural convection in these types of engineering flows due to their complex physical mechanisms therefore experimental investigations were often used. A closed rectangular cavity with an aspect ratio 5 between its height and width were studied by [2] in which temperature and velocity profiles were measured at the mid height of the cavity. Similar investigations for temperature distribution and local heat transfer rate in a rectangular cavity were also performed by [3] and [4]. Among these works the natural convection heat transfer was studied by varying the surface temperature differences between cavity walls. The inner surfaces of these testing rigs were made by aluminium alloy plate which tends to have a small emissivity (normally less than 0.1) therefore the heat transfer within the cavity was dominated by natural convection, and with the given temperature difference radiation effects from the internal walls were not examined. However, the surface radiation flux between cavity walls may have an impact on the temperature and velocity distribution when the inner surfaces of the cavity have a relatively large emissivity. The experiments of [5] were conducted on a square cavity with differentially heated vertical walls. The inner surfaces of the cavity were made by steel plates. In average the emissivity

^c Corresponding Author: Y.Ji

Email: y.ji@salford.ac.uk

Telephone: +44 116 295 4841

Fax: +44 116 295 4841

© 2014 All rights reserved. ISSR Journals

PII: S2180-1363(14)6015-X

of steel plate ranges from 0.7 to 0.8. With a 40 degree temperature difference between the hot wall and the cold wall, radiation effect may not be ignored for this case. The work of [6] investigated natural convection heat transfer and surface radiation in a three dimensional tall cavity with an aspect ratio of 16 between the height and width of the cavity. In the experiments both temperatures and emissivities of cavity wall surfaces were varied in order to quantify the convective and radiative heat fluxes of cavity wall surfaces. It is worth to note that there were cases in [6] the radiative heat fluxes were larger than the convective heat flux.

Cavity air flow and heat transfer were also investigated extensively using computational fluid dynamics (CFD). With the recent advances in computing power, the process of creating a CFD model and analysing the results is much less labour-intensive, reducing the time and therefore the cost. Some parameter investigations like change of geometrical factors, change of boundary conditions, which may be difficult to perform by using experimental studies, could be introduced using CFD modelling. Examples of CFD studies include the work of [7-10]. Among these studies, researchers were focusing on solving the natural convection heat transfer and/or radiation in different kind of cavities using different turbulence models, showing the capability of a specific model for specific cases. The current investigations are to evaluate the relative accuracy for the widely used turbulence models in engineering practices when modelling natural convection heat transfer with or without radiation in three typical cavities. Comprehensive details for using the turbulence models are presented and the modelling results are compared with the available experimental measurements, through which we may identify which model will be the better suited model for these types of airflows.

2. Experiments

Figure 1 shows the closed 2D cavity from [2] where only natural convection was considered (Fig 1a), the closed 2D cavity from [5] and the open-ended 3D cavity from [6] where both natural convection and radiation were considered (Figs 1b & 1c).

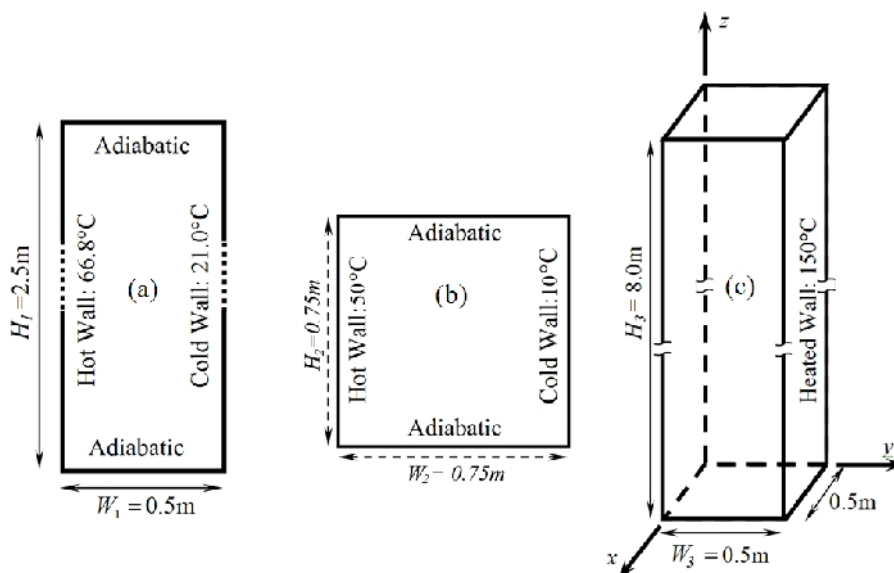


Figure 1. (a) 2D rectangular cavity, (b) 2D square cavity and (c) 3D tall cavity

In the study of [2] the aspect ratio of height and width was 5.0 with a 45.8 °C temperature difference between the hot and the cold aluminium alloy walls. The top and bottom of the cavity were well insulated and the heat losses and gains were ignored. The depth of the cavity was sufficiently long so that in the central region of the depth the airflow could be assumed to be two dimensional. A square cavity (aspect ratio is 1.0) was used in [5] and the temperature difference is

40°C between the two vertical steel plate walls. Other setups were similar with [2] in order to achieve a 2D flow at the centre of the testing rig.

The open-ended cavity of [6] has an aspect ratio of 16. The cavity comprised a heated wall at $y=0.5\text{m}$ and well insulated walls at $y=0$, $x=0$ and $x=0.5$ (Fig 1c). The top and bottom of the cavity are free openings which allow air to flow freely in any direction. In the experimental work, the emissivities of the cavity walls can be adjusted in order to examine the effects of radiation on the buoyancy-induced natural convection flow, and the heated wall temperature can be fixed at any value in the range of 100°C - 175°C. In this work the experimental measurements for the hot wall with emissivity of 0.9 and temperature of 150°C were used to compare with the CFD predictions.

3. CFD Modelling

The commercial CFD code Ansys CFX [11] was used to model the natural convection airflows for the cases described in section 2. Two equation eddy-viscosity turbulence models are investigated in this work. They are k-epsilon based models: the standard k-epsilon model [12] and the RNG k-epsilon model [13] and the k-omega based models: the k-omega model [14] and the Shear Stress Transport (SST) model [15]. These turbulence models offer a good compromise between computational cost and accuracy, and are applicable to investigate engineering cavity flows such as Trombe walls, solar collectors/chimneys, and double skin façades. The applications of these technologies in buildings are gaining popularity in recent years with the focus of reducing building carbon emissions [16, 17].

For steady-state natural convection applications, the two-equation models are formulated from the incompressible form of Reynolds Averaged Navier-Stokes (RANS) equation using the turbulent eddy-viscosity concept. The formulations of the eddy viscosity turbulence models have been well reported therefore not introduced here. For details please refer either [11] or [18] where the detailed derivations of these models are available

3.1. Modelling of the 2D cavities

For the rectangular case, wall boundary with fixed temperatures (66.8°C and 21°C, Figure 1a) is used for left and right walls and symmetry plane boundary is used at front and back in order to perform 2D calculation. The top and bottom of the cavity are modelled as adiabatic walls.

Simulations use time steps to reach their steady-state in CFX. These time steps do not define a transient flow so do not have to be uniform. In fact, the time steps should be as large as possible without causing the solution process to become unstable. For buoyancy-driven airflows, the time step size can be estimated using a relationship $\Delta t_{\max} = (L/(\beta g \Delta T))^{1/2}$ [11], where L is a length scale, β is the thermal expansion coefficient and ΔT is a temperature variation of the fluid. Δt_{\max} is about 1.3s for the case of [2]. Higher values (5.0s) were used to speed up the calculation and a value of 1.0s was used for finding the final converged solution.

Similar modelling routines were employed for the square cavity case. In this case the optimised time step is 1.25s. Due to the high emissivity of the internal finishes of this testing rig, radiation modelling was considered. A value of 0.75 was used for the emissivity of inner steel plate walls.

The convergence criteria for both cases are: i) all the maximum residuals are lower than 5×10^{-4} for the last 100 time steps and ii) the global domain imbalance for energy equation is less than 0.1%.

3.2. Modelling of the 3D cavity

The modelling methods used in the 2D cases are all applicable for the 3D case with the following differences: Except the heated wall (Figure 1c) with fixed temperature all other vertical walls are simulated as ‘adiabatic’ due to the well insulated condition for them. The top and bottom of the cavity are ‘opening’ boundaries which allow air to flow freely in any direction according to the pressure difference across the openings. In practice when fluids flow through sharp openings there will be losses in volume flow rate due to expansion or discharge of fluid flow at these openings. The losses can be represented by the loss coefficient f . A value of 2.4 was used for this study to estimate the pressure loss across the opening boundaries by a relation of $\Delta P_l = f\rho U_n^2 / 2$ (where U_n is the normal component of velocity).

Due to the high emissivities (0.9) of vertical walls and the large temperature differences between them, surface thermal radiation effects were taken into account for the CFD simulation. Thermal radiation model used in this research is the Monte Carlo (MC) Model. This model has wider engineering applications, particularly for radiation modelling in participating media and multi-domains with both transparent fluids and semi-transparent solids, such as airflow in glasses with external solar radiation [19].

4. Mesh and its dependency test

Figure 2 shows the structured surface mesh for the 2D closed rectangular cavity of [2] and the 3D open ended cavity of [6]. The mesh for the square cavity is similar as the rectangular cavity with the same mesh density for the top and bottom walls. Due to the high aspect ratios of these geometries, only the upper parts of the geometries are shown here.

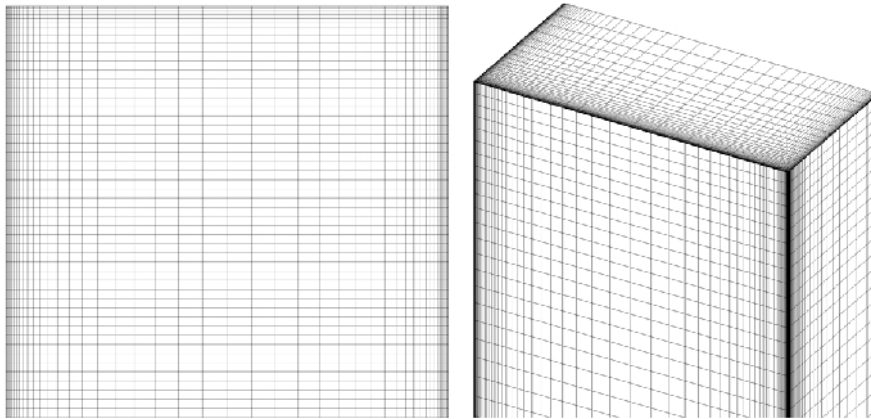


Figure 2 CFD surface meshes: (left) 2D rectangular cavity case and (right) 3D open ended case.

Mesh dependency investigations were conducted using k-omega turbulence model for the 2D rectangular natural convection cavity. Mesh1 uses 3000 elements (25×120) with the first cell to wall distance 2.5mm. Mesh2 uses 12500K elements (50×250) with the first cell to wall boundary distance 1.0 mm. Mesh3 uses 28125 elements (75×375) with 0.5mm first cell to wall distance. The resulting velocity and turbulence kinetic energy profiles at the mid height of the cavity are shown in figures 3a, b. The velocity profiles for the three mesh sizes show negligible differences while the turbulence kinetic energy profiles show small differences (less than 5%). Vertical temperature profiles of the three meshes at the centre of the cavity were also examined. Mesh1 shows differences compared with Mesh2 and Mesh3 (figure 3c). Although the velocity, temperature and turbulence kinetic energy profiles are not sensitive to the mesh densities and the first cell height, the local wall convective heat flux shows significant dependency with both mesh density and the first cell height at the lower region of the cavity (figure 3d). Clearly, Mesh1 results in a lower average

wall heat flux, while the predictions of Mesh2 and Mesh3 are similar. A new mesh structure Mesh4 was also tested. Mesh4 has the same cell numbers as Mesh2 (12500 cells) but has the same first cell height as Mesh3 (0.5mm). The resulting wall heat flux profile is overlapping on the Mesh3 profile. This indicates that increasing the mesh size with the same first cell height does not significantly change these parameters of interest therefore Mesh4 is used and its CFD modelling results are presented in section 5.

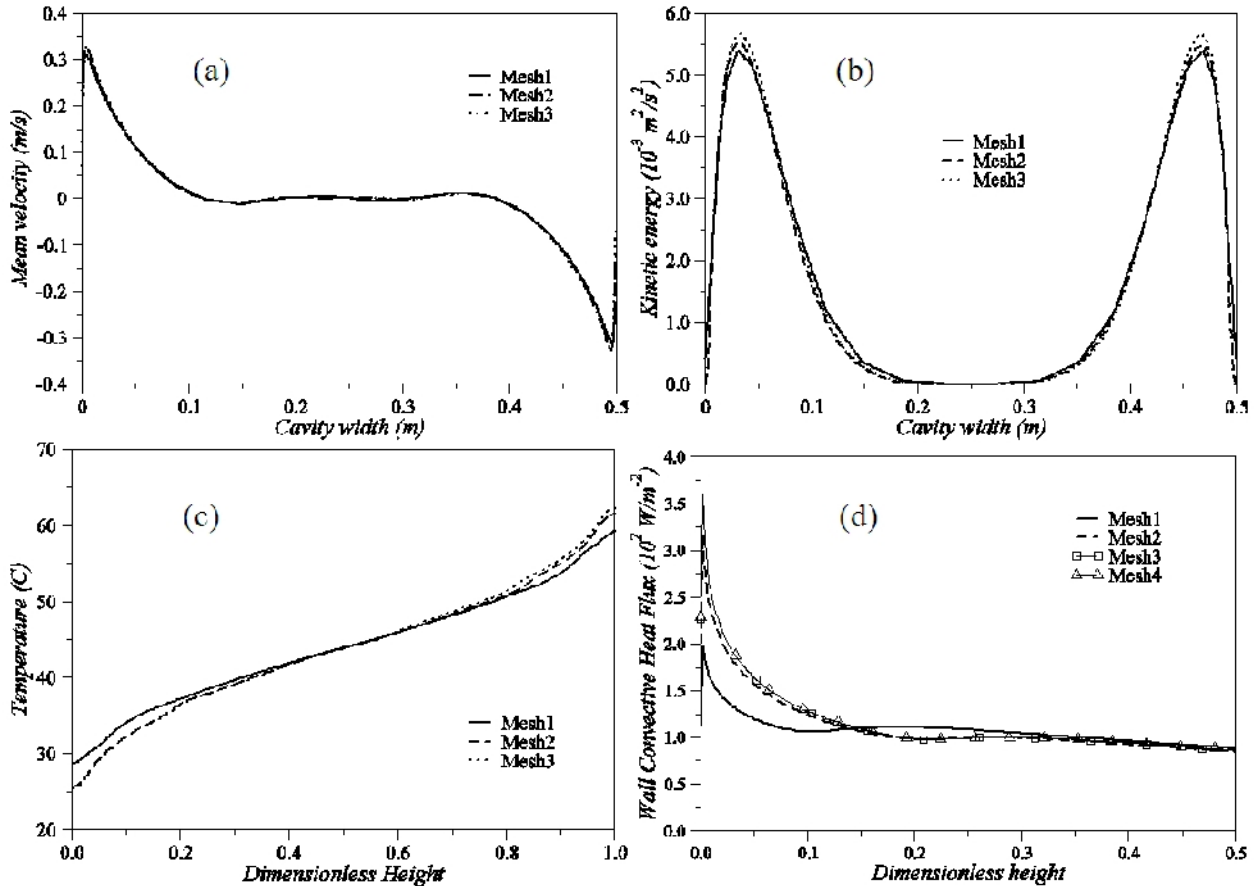


Figure 3 Mesh dependence test, (a) velocity and (b) turbulence kinetic energy at the mid height of the cavity; (c) vertical temperature profile in the core region and (d) wall convective heat flux along the hot wall.

Similar procedures were also performed for the cases of [5, 6]. The resulting structured mesh for the square cavity is 15625 cells with a first cell height of 0.5mm. The resulting mesh for the 3D case is 362,880 cells and 0.25mm first cell height bears both numerical consistency and accuracy. A smaller first cell height for the 3D case is needed compared with the 2D cases because of the higher aspect ratio and the larger temperature difference. The resulting local Reynolds number close to walls will be higher due to the potential higher convection air flow speed next to the walls, which potentially leads to a thinner viscous sub-layer for the 3D case. The resulting average/maximum Y_{plus} (dimensionless wall distance) values for Mesh4, the mesh used for the square cavity and the mesh used for the 3D cavity are 1.61/3.03, 1.42/2.57 and 1.53/2.98 respectively. Figure 4 shows the Y_{plus} contour with rounded maximum on the relevant solid walls. Only part of the wall surfaces were shown due the single cell depth (for the 2D cases with symmetry boundaries) and the aspect ratio (i.e. the 3D case). The average of Y_{plus} is across the whole surface in question. The mesh densities for all three cases are acceptable for the turbulence models studied in this work [11].

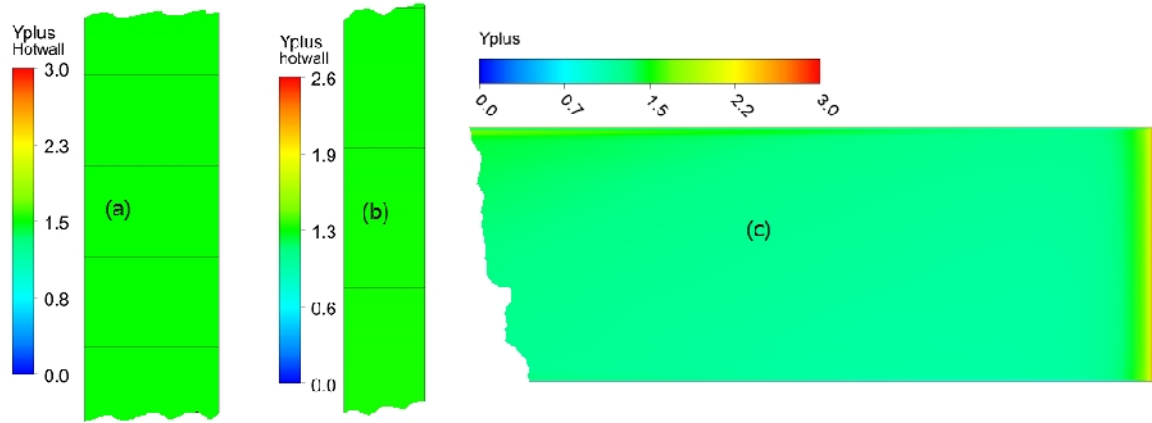


Figure 4 Yplus plots Cheesright case Mesh 4 (a), square cavity (b) and the 3D cavity (c).

5. Results and discussions

5.1 Two dimensional rectangular cavity

The temperature contour of the cavity shows that the air flow inside the cavity was strongly stratified due to the asymmetrical boundary conditions of hot and cold walls (figure 5a) which gives a relatively linear temperature gradient in the core region along the vertical height. The gradient is slightly increased at the upper and lower ends. This is consistent with the temperature profiles shown in figure 3c. The velocity vector shown in figure 5b is on a sample plane which does not reflect the real mesh information (the plots on the real mesh will be too dense to display properly). It simply shows the strength of air movement within the domain. At centre region of the mid height (also away from the wall boundaries) of the cavity the airflow shows the least motion due to the effects of the upstream and downstream close to the hot and cold walls (figure 5b). This is consistent with figure 3a.

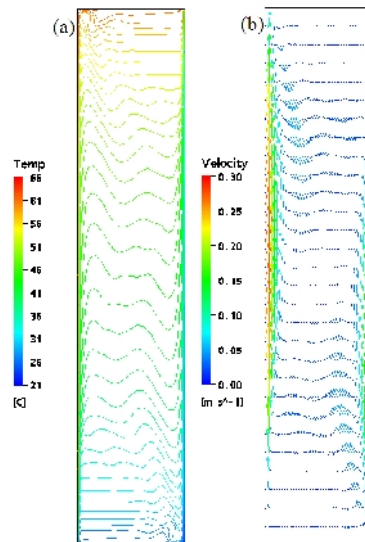


Figure 5 Temperature field (a) and velocity vector (b) inside the cavity of the 2D case.

The turbulence diffusive potential is often measured by the turbulence viscosity within the flow field, while the turbulence viscosity is determined through turbulence modelling. Higher turbulence viscosities will increase the turbulence diffusivity and potentially increase the thickness of the boundary layer. Figure 6 shows the scaled

turbulence viscosity (STV, turbulence viscosity over the molecular dynamic viscosity μ_t / μ) predicted by the different turbulence models. A relatively large turbulence region was predicted by the k-omega and k-epsilon models. The k-omega model gives the highest turbulence viscosity among the four models. The differences on the predictions of turbulence viscosity and other parameters (table 1) between these models may be caused by their individual modelling method for turbulence. In order to assess the accuracy of these models, the simulation results are further compared with other quantitative data collected from the experiments.

TABLE 1 PREDICTIONS OF TURBULENCE AND HEAT TRANSFER PARAMETERS

	k-omega	SST	k-epsilon	RNG
Average μ_t / μ	9.5	3.62	9.12	4.99
Maximum μ_t / μ	43.4	23.8	34.2	24.9
Average heat flux on Hotwall (W/m ²)	84.7	81.6	45.8	42.7
Average kinetic energy k (10 ⁻³ m ² /s ²)	1.08	0.60	0.70	0.60

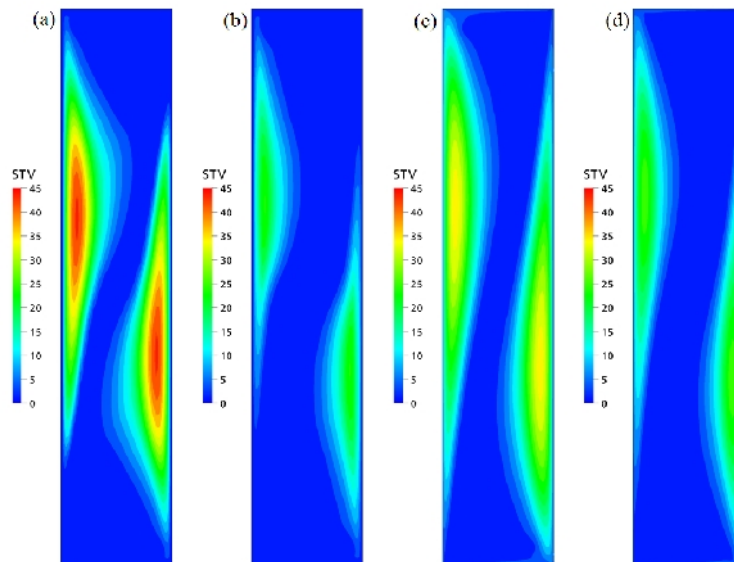


Figure 6 Scaled turbulence viscosity contour predicted by (a) k-omega model, (b) SST model, (c) k-epsilon model and (d) RNG k-epsilon model.

Figure 7 shows that the vertical temperature along the centre of the cavity was over-predicted by all four turbulence models above one-fifth of the cavity. Ideally, the cross point of the mid height and mid width of the cavity would have the averaged temperature of T_h and T_c when all the wall boundaries are ‘adiabatic’ or ‘adiabatic’ with a fixed temperature. This is the case for all four turbulence models (the cross point in figure 7, the non-dimensional height and the non-dimensional temperature, both at 0.5) but is not the case for the measurements (the non-dimensional temperature is about 0.41). This implies that the measurements inside the cavity were lower than expected due to the heat loss through the insulation. The high loss would be expected at the upper end of the cavity because the higher temperature gradient there. It is difficult to justify the performance of these turbulence models through this temperature measurements because a more realistic boundary condition for walls may be needed, for example, giving a non-linear heat loss boundary for side walls and giving the top and bottom ‘walls’ a temperature profile with edge effects like the method used in [20]. This is not further discussed in this paper due to the lack of boundary information for the experiments.

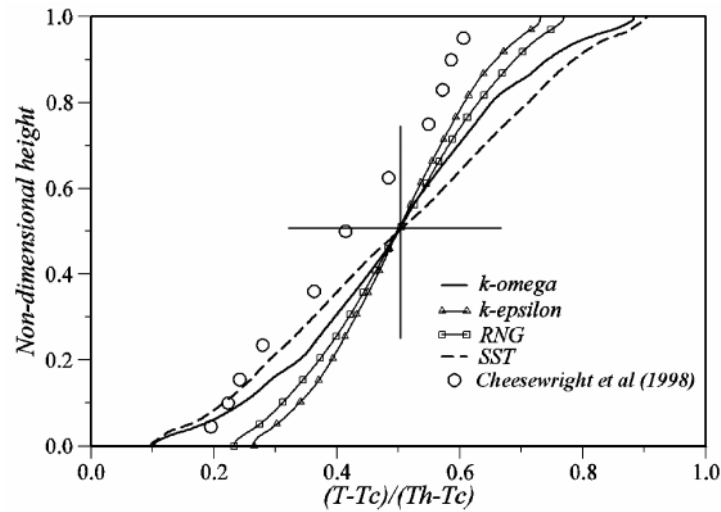


Figure 7 Predicted and measured temperatures along a vertical height at the middle width

Figure 8 shows the comparisons between the CFD predictions and the experiments for the mean velocities at mid height of the cavity (across the cavity width). These mean velocity data used here were not the direct measurements from the experiments but the data which have been corrected from the potential three dimensional effects and the possible effects of heat losses through imperfect wall conditions for validation purposes [2]. Qualitatively, all four turbulence models agree with the experimental data. That is, they show the large mean positive velocity close to the hot wall, large mean negative velocity close to the cold wall, and the relatively stagnant core in the centre region of the cavity. Within the boundary regions of the hot and cold walls, the SST model over-predicts the maximum mean velocity and under-predicts the thickness of the boundary layer; while the k-epsilon and RNG models under-predicted both the maximum mean velocity and the thickness of the boundary layer close to walls. Overall, close agreement was achieved by k-omega turbulence model for predicting the mean velocity across the cavity at the mid height.

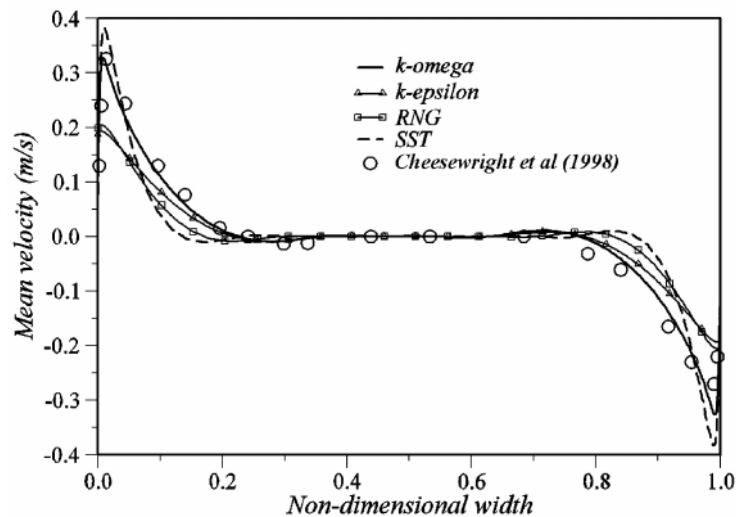


Figure 8 Predicted and measured mean velocities at the middle height across the cavity width

The CFD predictions of the turbulence kinetic energy at the middle height of the cavity are compared with the experimental measurements (corrected similarly like the mean velocity for validation purposes) in figure 9. In general, the peak of this parameter was under-predicted by all the turbulence models although the four models had similar performance in the core region of the cavity at this height. The boundary thickness of the

kinetic energy close to wall was under-predicted by the SST turbulence model due to the fast dissipating of the turbulence eddies, which leads to lower turbulence intensity predicted by this model. The k-epsilon based model failed to resolve the wall boundary properly for this case. The k-omega model gives a reasonable agreement except the maximum turbulence kinetic energy.

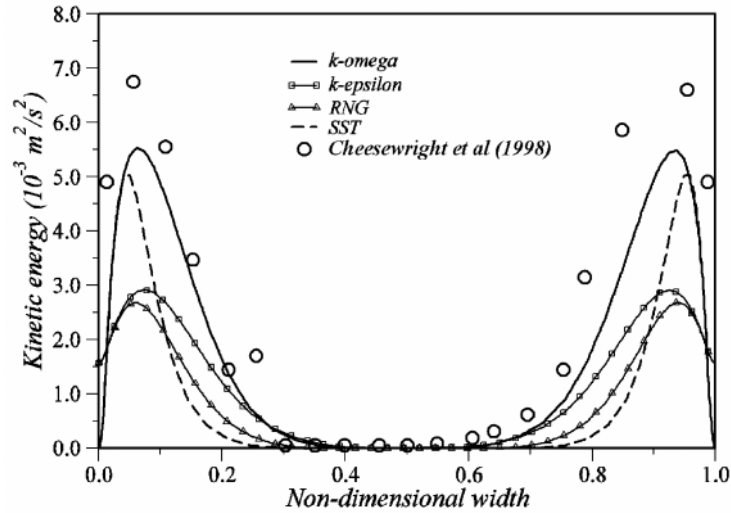


Figure 9 Predicted and measured kinetic energy at the middle height across the cavity width

Figure 10 shows the local convective heat flux predicted by different turbulence models along the heated wall surface. The predicted transient onsets (shown as the upper turning points for the local convective heat flux in figure 10) for the k-omega and SST models are at 0.21 to 0.24 (dimensionless height), while the experiments gave a value of 0.22 [21]. This implies that the k-omega based turbulence models gave reasonable close prediction for the convective heat transfer and the transition onset. However, lower convective heat fluxes were predicted by the k-epsilon based turbulence models and the transition onsets were not clearly identifiable.

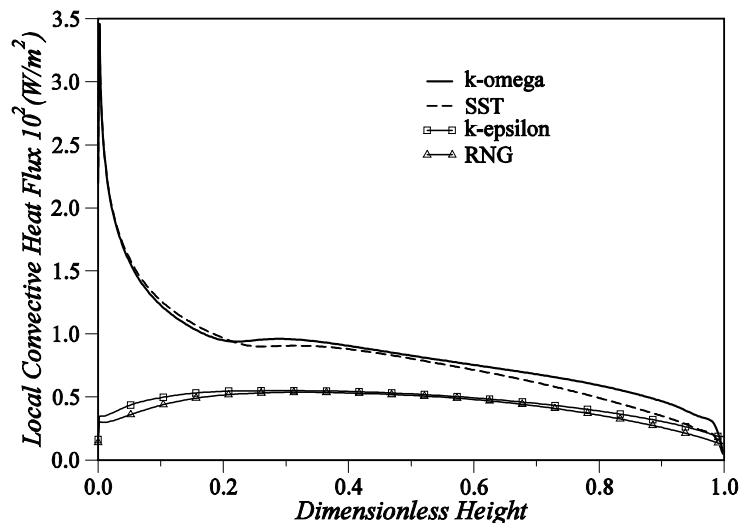


Figure 10 Predictions of the local Nusselt number along the heated wall surface.

5.2 Two dimensional square cavity

The principle and modelling approach for this case were both similar as the rectangular case apart from the involvement of radiation modelling. The predicted

temperature at mid-width of the cavity is shown in figure 11. Clearly, k-omega model with radiation modelling, the temperature profile is much improved compared with the modelling result without radiation referencing the experimental measurements. The accuracy of SST model with radiation is reasonable but not as good as k-omega model for this case. While the other two k-epsilon based models showed large discrepancies with the measurements.

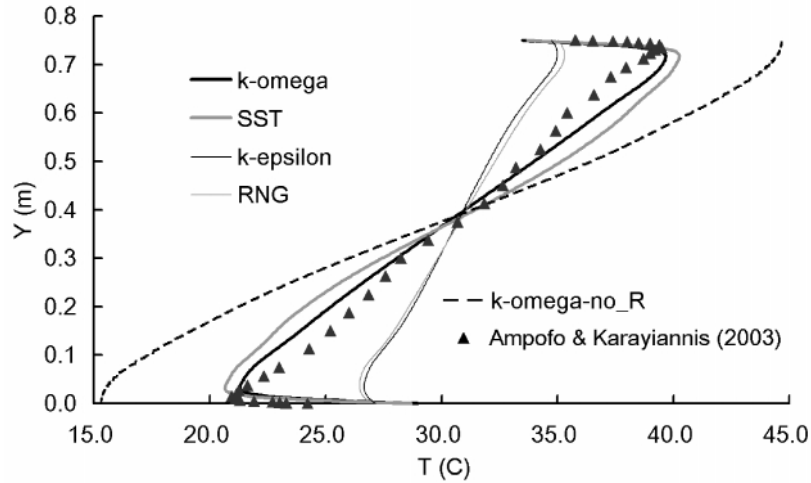


Figure 11 Vertical temperature profiles at mid-width of the cavity (the dashed line is the prediction of k-omega model without radiation)

Figure 12 shows the temperature contour of both with and without radiation modelling for this square cavity using k-omega model. Without radiation model, the stratifications are relatively uniform as numbered on the image; while for the modelling with radiation, the top and bottom walls are able to absorb radiative heat from surroundings and the increased surface temperature will intensify the convective heat transfer between their surfaces and surrounding air. For the case without radiation modelling, the surface temperature of the top and bottom wall tends to be the same as the surrounding air, convective heat transfer is kept to the minimum (may only happened at the upper left and the lower right corners). This explains why the temperature profiles of k-omega model in figure 11 are so different for ‘with and without radiation’ modelling. On figure 11, temperature profiles without radiation modelling for turbulence models other than k-omega model are not shown because they have the similar level of difference as illustrated by k-omega model.

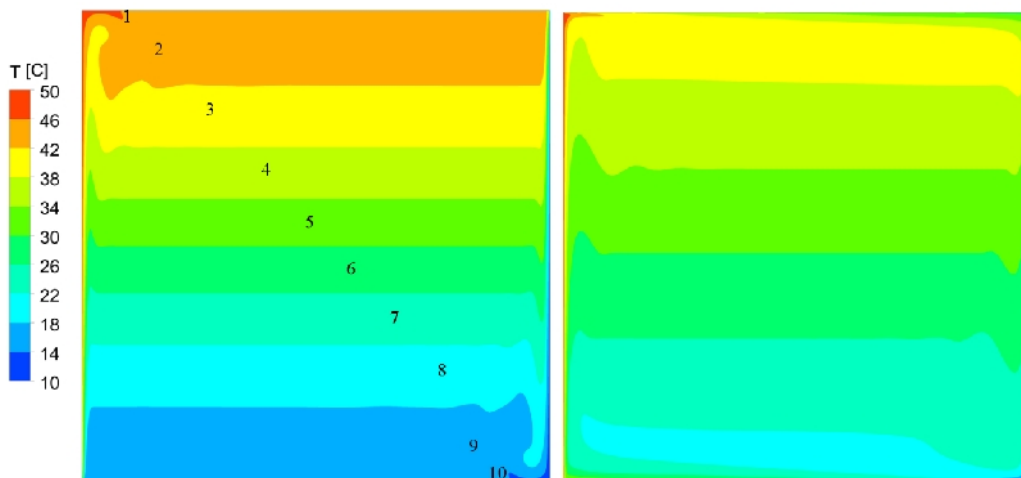


Figure 12 Temperature contour predicted by k-omega model for the square cavity case: without radiation modelling (left) and with radiation modelling (right).

Figure 13 shows the mid-height vertical velocity profiles predicted by the four turbulence models in comparison with the experimental measurements. The detailed measurements were conducted from the ‘hot’ wall side till the vertical velocity variation gets steady and close to zero. Both RNG and k-epsilon model failed to perform at the boundary inner layer and the predictions of the outer layer are poor, too. SST model resolved the inner boundary similar as the k-omega model but had an overshoot of the maximum vertical velocity and consequently a relatively thinner outer boundary layer compared with both k-omega model and the measurements. Overall, k-omega model performs better here. Without the radiation model involved, all the models failed to predict the boundary layer next to the hot wall. On figure 13, only k-omega model resulted profile without radiation is shown.

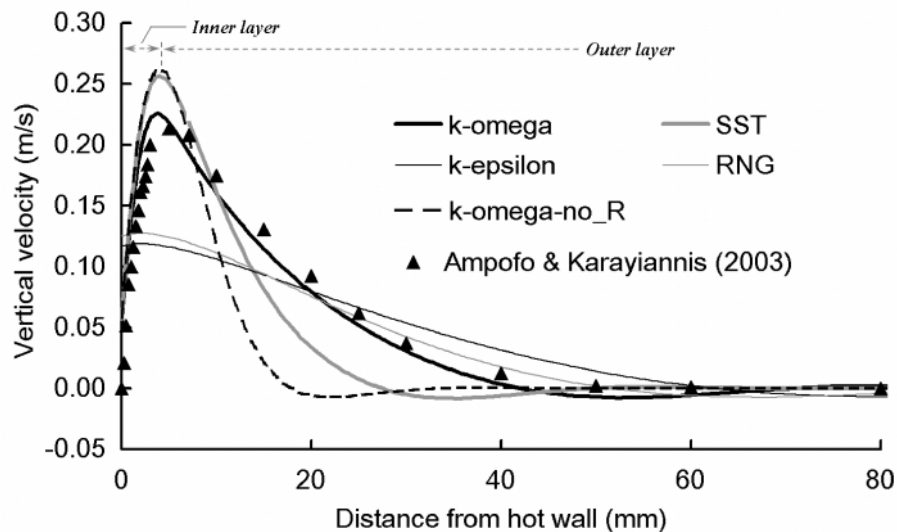


Figure 13 Vertical velocity profiles at mid-height close to the hot wall (the dashed line is the prediction of k-omega model without radiation)

Although the four turbulence models are using the same eddy viscosity assumption (Reynolds stresses are assumed to be proportional to mean velocity gradients) for representing the turbulence viscosity μ_t , the near wall treatments for these models are different, which may have led to the differences of their predictions. The k-epsilon based models use a ‘scalable wall function’ in which a lower limit for the first cell height close to wall was set. This is the height at the intersection of the logarithmic and the linear near-wall profile. In this approach the viscous sub-layer is bridged by employing empirical formulas to provide near-wall boundary conditions for the mean flow and turbulence transport equations. Therefore all cells within the computing domain are outside the viscous sub-layer and this avoids the inconsistency caused by arbitrarily fine meshes. This wall function works well for buoyancy-driven natural or forced convection in enclosed spaces when the buoyancy turbulence is caused by localised heat sources [22, 23]. However, for the cases considered here, the buoyancy driving force is generated by the differentially heated surfaces. Parameters like wall heat transfer and shear stresses in the viscous sub-layer are very sensitive with the near-wall formulation. It may not be appropriate using an empirical logarithm profile outside the layer. The differences between the k-epsilon model and the RNG model are that the RNG model uses the renormalisation group analysis for the Navier-Stokes equations and also uses different model constants for the turbulence transport equations. The RNG model performs better than standard k-epsilon model when turbulence buoyant plume is modelled [22-24].

The near-wall treatment for the k-omega based models is using the formulation for low-Reynolds number computations. However, the k-omega models do not involve the complex non-linear damping functions required for the k-epsilon model and are therefore more robust. The models allow for smooth shift from a low-Reynolds number form to a wall function formulation. The SST k-omega model gives highly accurate predictions of the onset and the amount of flow separation under adverse pressure gradients because it accounts for the transport of the turbulent shear stress [15]. In this work, the airflow cavity does not involve the complicated flow structure like separation and reattachment. For this reason the SST model did not offer more accurate prediction than the k-omega model of [14].

5.3 Three dimensional cavity predictions

Figure 14 shows the velocity and temperature predictions on the mid plane ($y=0.25\text{m}$) by k-omega turbulence model. There are about 10 to 12 cells to resolve the viscous sub-layer and this gives a smooth shift from the viscous layer to the turbulent region. The maximum speed after the viscous layer is about 1.5m/s on the mid plane and the highest (about 2.44m/s) speed is located close to the outlet of the cavity. This explains why a smaller first cell height is needed compared with the 2D case where the resulting air speed near wall was small. The thickness of the thermal boundary layer increases with height and towards the top of the cavity the thermal boundary layers are interacting from one side to the other. This is also shown by the velocity profiles at locations (1, 2, 3) because the effects from the boundary layer have propagated to the centre at the top of the cavity.

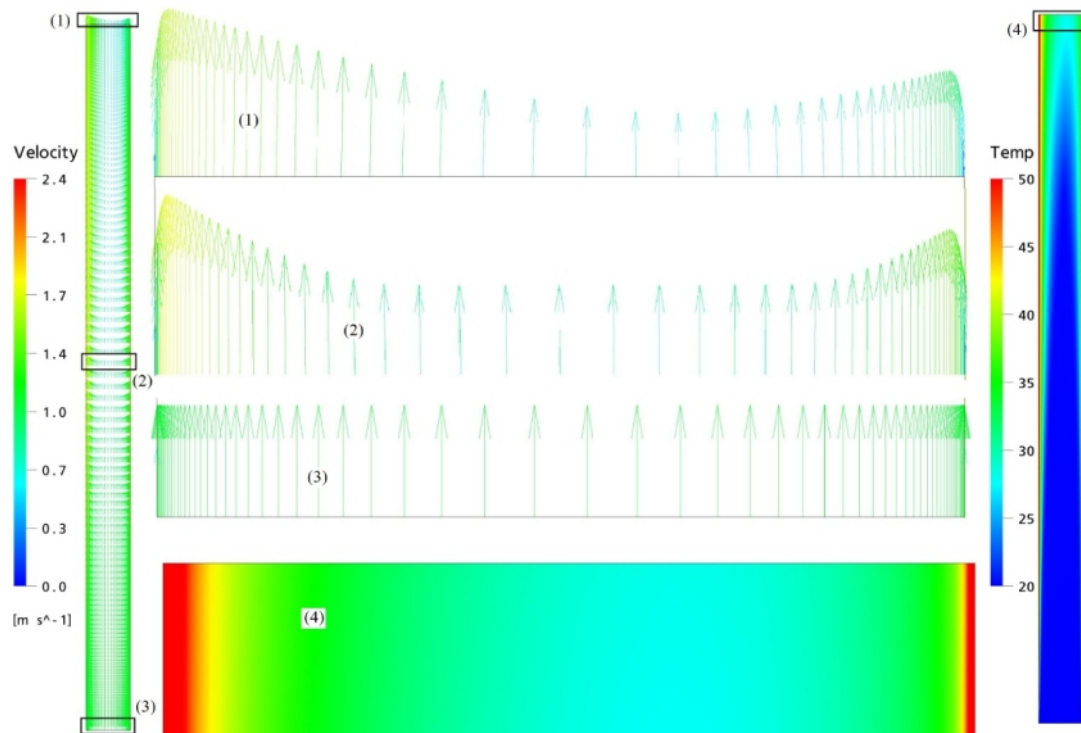


Figure 14 The velocity vectors and temperature contours on the symmetry plane ($y=0.25$).

Figure 15 shows the CFD predicted air velocity profiles at a height of 7.8m compared with the experimental measurements [6]. The SST model predicted a higher mean velocity at the boundary region. However, the effects of this high momentum are quickly

dissipated and do not seem to adequately affect the flow in the core of the cavity, where the air tends to be stagnant. Predictions from the other three models agreed with the measurements in general with the k- ω model performed slightly better at both near-wall region and the core flow. This is also true for the prediction of the temperature profile at the same location (Figure 16).

The temperature profile predicted by the four turbulence models all follow the trend of the experiments but the predictions are all slightly higher than the measurements (Figure 16). Again, the predictions of k- ω model are slightly closer to the experiments. The over predictions of this temperature profiles may be caused by the relative portion of the radiative energy and the convective energy on the heated wall. A relative higher portion of convective heat was predicted by all four turbulence models (table 2) and this heat has been taken away by air due to convection which may have increased the air temperature within the cavity. The mass flow rates predicted by CFD are all slightly smaller than that in [6] which may contribute another reason for the over-predictions of air temperature profile.

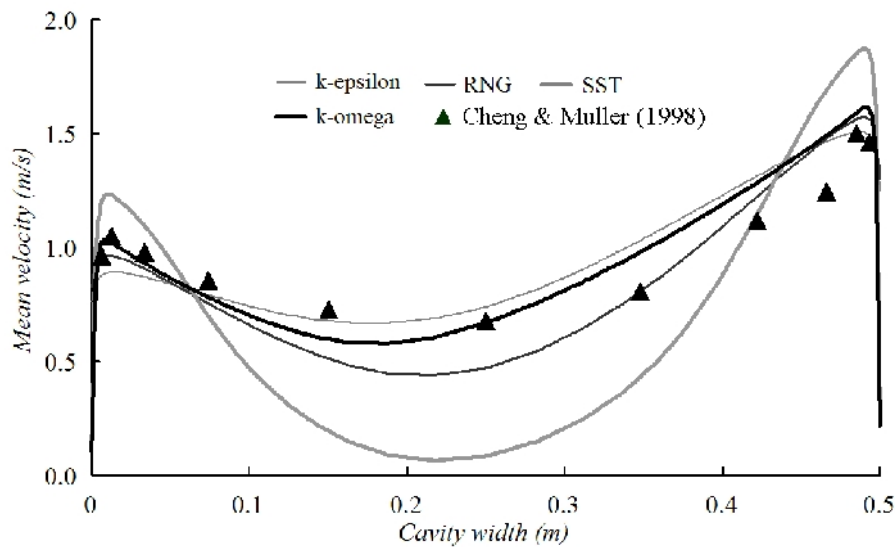


Figure 15 Comparisons between CFD and experiments for the prediction of velocity profiles at $H=7.8\text{m}$ across the symmetry plane.

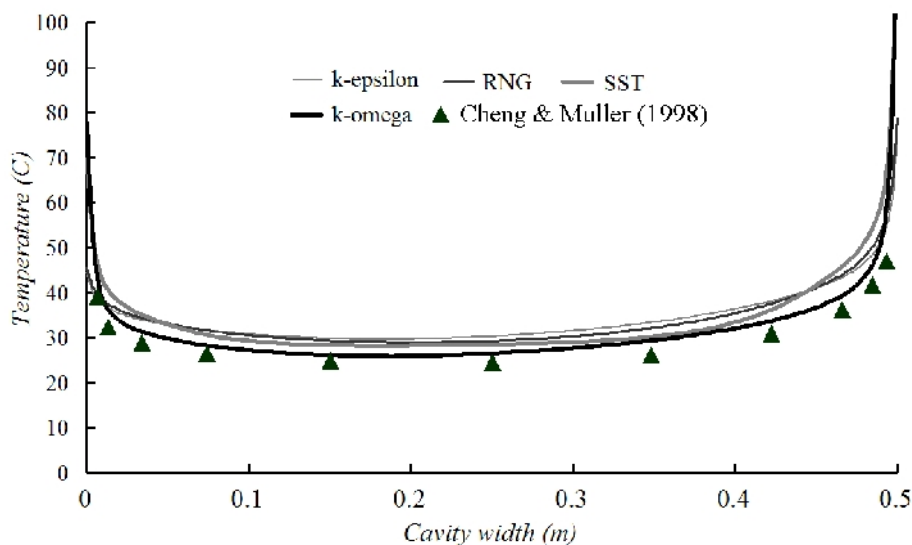


Figure 16 Comparisons between CFD and experiments for the prediction of air temperature at $H=7.8\text{m}$ across the symmetry plane.

Table 2 shows the comparisons between the experiments and the CFD predictions for 5 other parameters. The total heat flux is the overall heated wall energy output which included both convective and radiative heat. When the heated wall is set to 150°C the measured total heat fluxes were tending to towards the lower band therefore all the CFD predictions agreed with the measurements closely [6]. As discussed previously, all turbulence models predicted a slightly smaller ratio of radiative heat over convective heat compared with experiments, which is also true for the predictions of the mass flow rate. This discrepancy may be caused by the radiation modelling where the radiative heat may be under-predicted. The under-prediction of mass flow rate may be caused by loss coefficient imposed on the open ends, a smaller resistance than the current simulation setup may be needed to overcome this. The CFD predicted local Nusselt numbers on the heated wall for convective and total energy are also compared with the experiments. The predictions all fall in the range of the experimental measurements which indicates that all turbulence models performed well with this parameter. However, there is a clear distinction between k-omega and k-epsilon based models. The difference is considered to be caused by the near-wall treatment for these turbulence models, e.g. the scalable wall-function is used by the k-epsilon based models while the k-omega based models use automatic near-wall treatment which automatically switches from wall-function to a low Reynolds number formulation at the viscous sub-layer. Further discussions for these near-wall treatments and how these Nusselt numbers are calculated can be found in Appendix A.

TABLE 2 COMPARISONS BETWEEN TEHEXPERIMENTS AND CFD PREDICTIONS

	Total heat flux	q_r / q_c	Flow rate	Nu_c	Nu_t
Measured	6.60±10% (KW)	1.25	0.34 (kg/s)	112.2±10%	
k-epsilon model	6.24 (KW)	1.10	0.32 (kg/s)	132.2	277.6
RNG model	5.96 (KW)	1.16	0.30 (kg/s)	128.1	276.7
SST model	6.04 (KW)	1.11	0.27 (kg/s)	102.9	217.1
k-omega model	6.22 (KW)	1.14	0.32 (kg/s)	106.9	228.8

Key: q_r , and q_c are radiative, convective heat on the heated wall and Nu_c and Nu_t are the convective and total Nusselt Numbers which are defined in Appendix A.

6. Conclusion

This paper has demonstrated the ability of four widely eddy viscosity turbulence models for modelling natural convection airflow in closed and open ended cavities with and without radiation. Modelling techniques were detailed and the grid dependency was performed for all three cases. Simulation results have been compared with their corresponding experimental measurements. The four turbulence models performed differently when predicting key parameters of interest.

The k-epsilon based models resolved much lower peaks of mean velocity and kinetic energy at near-wall region for the 2D rectangular closed cavity case although the predictions of the core region agreed with experiments well. This is also true for the squared cavity with radiation modelling in the prediction of the mid-height velocity. The two k-epsilon based models were not able to predict location of the transient onset, which is identified as the upper turning point for the local convective heat flux on the hot wall for the 2D rectangular case. When modelling the open-ended 3D case in conjunction with radiation k-epsilon based models performed better for the prediction of the near-wall velocity field and the heat transfer parameters compared with the 2D cases. The k-omega based models were able to accurately predict the transient onset and resolved higher peaks of the mean velocity and kinetic energy for the rectangular 2D case. Similarly for the square 2D case with radiation, the k-omega based models performed better than the other two

models. However, the SST model over-predicted the peak velocities and resolved a thinner boundary layer for all three cases compared with experiments and other turbulence models. The thin boundary layer for the SST model has contributed the under-prediction of the velocity field at the core region of the 3D case. On the predictions of both velocity field and near-wall heat transfer parameters the k-omega model agreed with experiments closely. In the 3D case, the temperature fields were all over-predicted by the four turbulence models tested with k-omega model performed slightly better than others. Overall, the predictions from the k-omega model agreed with experiments better than other models for the three typical cavity cases investigated.

REFERENCES

- [1] Short C.A., Cook M., Lomas K.J. (2009) ‘Delivery and performance of a low-energy ventilation and cooling strategy’, *Building Research and Information*, 37 (1), pp. 1-30. <http://dx.doi.org/10.1080/09613210802607841>
- [2] Cheesewright R, King KJ and Ziai S (1986). Experimental data for the validation of computer codes for the prediction of two-dimensional buoyant cavity flows. *Proceedings of the ASME Meeting, HTD. 60*, 75-81.
- [3] Cheesewright R and Ziai S (1986). Distributions of temperature and local heat transfer rate in turbulent natural convection in a large rectangular cavity. *Proceedings of the 8th International Heat Transfer Conference, San Fransisco*, pp 1465-1470.
- [4] Wu W, Ewing D and Ching CY (2006). The effect of the top and bottom wall temperatures on the laminar natural convection in an air-filled square cavity. *International Journal of Heat and Mass Transfer*, vol. 49, pp 1999-2008.
- [5] Ampofo F and Karayiannis TG (2003). Experimental benchmark data for turbulent natural convection in an airfilled squared cavity. *International Journal of Heat and Mass Transfer*, vol 46, pp 3551-3572.
- [6] Cheng X and Muller U (1998). Turbulent natural convection coupled with thermal radiation in large vertical channels with asymmetric heating. *Int. J. Heat Mass Transfer. Vol. 41, No.12*, pp.1681-1692.
- [7] Colomer G, Costa M, Consul R and Oliva A (2004). Three-dimensional numericalsimulation of convection and radiation in a differentially heated cavity using the discrete ordinates method. *International Journal of Heat and Mass Transfer, Vol. 47*, pp. 257-269.
- [8] Ben Nasr K, Chouikh R, Kerkeni C and Guizani A (2006). Numerical study of the natural convection in cavity heated from the lower corner and cooled from the ceiling. *Applied Thermal Engineering (short communication)*, vol 26, pp 772-775.
- [9] Mezrhab A, Bouali H, Amaoui H and Bouzidi M (2006). Computation of combined natural-convection and radiation heat transfer in a cavity having a square body at its centre. *Applied Energy*, vol. 83, pp 1004-1023.
- [10] Gan G (2006). Simulation of buoyancy-induced flow in open cavities for natural ventilation. *Energy and Buildings*, vol. 38, pp 410-420. <http://dx.doi.org/10.1016/j.enbuild.2005.08.002>
- [11] Ansys CFX (2009). Version 12, user manual, www.ansys.com [Accessed: Dec 2012]
- [12] Launder BE and Spalding DB (1974). The numerical computation of turbulent flows. *Computer Methods in Applied Mechanics and Engineering*, vol. 3, pp 269-289.
- [13] Yakhot V, Orszag SA, Thangham S, Gatski TB and Speziale CG (1992). “Development of turbulence models for shear flows by a double expansion technique”, *Phys. Fluids A*, 4(7), pp. 1510-1520.
- [14] Wilcox DC (1986). Multiscale model for turbulent flows. AIAA, the 24th Aerospace Sciences Meeting. American Institute of Aeronautics and Astronautics.

- [15] Menter FR (1994). Two-equation eddy-viscosity turbulence models for engineering applications. *AIAA-Journal*, vol. 32(8), pp 269-289.
- [16] Stazi F., Mastrucci A. & Perna C. (2012). Trombe wall management in summer conditions: An experimental study, *Solar Energy*, Vol 86 (9), pp, 2839-2851. <http://dx.doi.org/10.1016/j.solener.2012.06.025>
- [17] Rodríguez-Hidalgo M.C., Rodríguez-Aumente P.A., Lecuona A. & Nogueira J. (2012). Instantaneous performance of solar collectors for domestic hot water, heating and cooling applications, *Energy and Buildings*, Vol 45, pp 152-160. <http://dx.doi.org/10.1016/j.enbuild.2011.10.060>
- [18] Versteeg HK and Malalasekera W (1995). An introduction to computational fluid dynamics – the finite volume method. ISBN 0-582-21884-5.
- [19] Ji Y, Cook MJ, Hanby VI, Infield DG, Loveday DL and Mei L (2007). CFD Modelling of Double-Skin Facades with Venetian Blinds. The 10th Int Building Performance Simulation Association Conf, 3-6 September, Beijing, China, pp. 1491-1498, ISBN: 0-9771706-2-4.
- [20] Hsieh KJ and Lien FS (2004). Numerical modelling of buoyancy-driven turbulent flows in enclosures. *International Journal of Heat and Fluid Flow*, Vol. 25, pp. 659-679..
- [21] Bowles A and Cheesewright R (1989). Direct measurement of the turbulence heat flux in a large rectangular air cavity. *Experimental Heat Transfer*, Vol. 2, pp. 59-69.
- [22] Cook MJ, Ji Y and Hunt GR (2003). CFD modelling of natural ventilation: combined wind and buoyancy forces. *International Journal of Ventilation*, Vol. 1, pp. 169-180.
- [23] Ji Y, Cook MJ and Hanby V (2007). Modelling of displacement natural ventilation in an enclosure connected to an atrium. *Building and Environment*, vol. 42, pp 1158-1172. <http://dx.doi.org/10.1016/j.buildenv.2005.11.002>
- [24] Chen Q (1995). Comparison of different k- models for indoor air flow computations. *Numerical Heat Transfer, Part B*, vol. 28, pp 353-369.

Appendix A: Nusselt Numbers on the heated wall for the 3D cavity

The measurement of local convective Nusselt number was correlated by the following equation:

$$Nu_c = 0.1Ra^{1/3} \quad (A1)$$

where, the Rayleigh number Ra is defined by equation A2

$$Ra = (\beta g l^3 \Delta T) / (\nu \alpha) \quad (A2)$$

The parameters at the average temperatures 30°C for equation A2 are shown in table A1 and these properties gave a Ra number as 1.41×10^9 .

TABLE A1 PARAMETERS FOR EQUATION A2

expansion coefficient β (1/K)	Gravity g (m/s ²)	Characteristic length l (m)	Temperature difference ΔT (K)	Kinematic viscosity ν (m ² /s)	Thermal diffusivity α (m ² /s)
0.00330	9.81	0.5	130.0	1.60×10^{-5}	2.29×10^{-5}

The total Nusselt number was defined by

$$Nu_t = Nu_c (1 + q_r / q_c) \quad (A3)$$

where q_r and q_c are the radiative and convective heat fluxes on the heated wall, which can be computed from the CFD directly.

The local convective Nusselt number at the heated wall in CFD can be defined by equation A4

$$Nu_c = \frac{(-\partial T / \partial y) l}{\Delta T} \quad (A4)$$

where $\partial T / \partial y$ is the temperature gradient related to the near-wall treatments for different turbulence models. In this work, ∂T is treated as the difference between the CFD calculated near-wall temperature and the boundary temperature, and ∂y is the normal distance from the heated wall where this near-wall temperature is calculated.

The key advantage of using scalable wall-function in the k-epsilon based models is to set a lower y^+ (dimensionless wall distance) limit as the intersection between the logarithmic and the linear near-wall profile which will avoid the mesh sensitivity close to the wall [11]. In this work, this limit is 11.6 because the meshes used have much smaller averaged y^+ values across the heated wall. Therefore the actual distance (Δy) between the heated wall and the intersection point can be obtained by the following equation:

$$y^+ = (u^* \Delta y) / \nu = 11.6 \quad (\text{A5})$$

where u^* is the near-wall velocity defined by

$$u^* = C_\mu^{1/4} k^{1/2} \quad (\text{A6})$$

where k is the kinetic energy which can be computed by CFD, C_μ is the model constant (RNG model $C_\mu = 0.085$ and k-epsilon model $C_\mu = 0.09$)

For k-omega based turbulence models, the automatic near-wall treatment was used. The near-wall temperature was calculated at the first cell height therefore Δy is the physical height of the first cell next to the heated wall.

The CFD computed ∂T and ∂y values used to calculate local convective Nusselt number are summarised in the following table A2

TABLE A2 ∂T AND ∂y VALUES CALCULATED BY THE TURBULENCE MODELS

	∂T (K)	$\partial y = \Delta y$ (mm)
k-omega	6.945	0.25
SST	6.689	0.25
k-epsilon	68.73	2.0
RNG	66.63	2.04